Fluid Dynamics &
Materials Processing

Tech Science Press

http://doi.org/10.32604/fdmp.2026.080083

ARTICLE

Perforated Partition Walls in Extra-Long Tunnels: A One-Dimensional Flow Model Based on Orifice Theory

Yunchao Du*, Xianming Shi, Zhiqiang Liu and Jian Wu

China Railway-Southwest Research Institute Co., Ltd., Chengdu, China
*Corresponding Author: Yunchao Du. Email: yunchao220225@163.com or duyunchao@crecg.com

Received: 02 February 2026; Accepted: 08 April 2026; Published: 07 May 2026

ABSTRACT: Perforated partition walls are widely employed in complex underground transportation systems to mitigate tunnel pressure waves, harness train-induced piston wind for reduced ventilation energy consumption, and support emergency operations. Building on orifice flow theory, this study develops a one-dimensional flow model for tunnels equipped with perforated partition walls. The model is applied to examine the aerodynamic performance of such walls in extra-long tunnels through a comprehensive parametric analysis, considering the presence of openings, opening ratio, spacing, and spatial arrangement. The results demonstrate that, for opening ratios, defined as the ratio of the perimeter of a single opening to the wetted perimeter of the tunnel on the train-passing side, ranging from 0 to 0.32, the model accurately captures train-induced pressure fluctuations. The introduction of a perforated partition wall reduces the overall amplitude of pressure fluctuations by 41.7% compared with the non-perforated configuration. Specifically, pressure peaks outside the leading and trailing cars decrease by 41.4% and 28.5%, respectively. Increasing the opening area enhances cross-wall airflow and effectively attenuates pressure fluctuations on the train-passing side, while reducing opening spacing further intensifies this effect. For a fixed number and ratio of openings, a uniformly distributed arrangement along the entire wall produces smoother pressure variations than configurations concentrated near the center or ends. An optimal design is identified, consisting of a uniform opening distribution with an opening ratio of 0.20 and a spacing of 10 m.

KEYWORDS: High-speed train; extra-long tunnel; perforated partition wall; pressure fluctuations; one-dimensional flow model

1 Introduction

Global high-speed railway networks are expanding rapidly, and urban underground space utilization is developing intensively. As a result, complex underground transportation infrastructures—such as long and large tunnels, underground stations, and multi-line parallel tunnels—have become increasingly common [1]. When trains travel at high speeds inside tunnels, a series of complex aerodynamic phenomena is induced. These include strong tunnel pressure waves [2,3], exit micro-pressure waves [4,5], significant aerodynamic drag [6], and intense piston wind effects [7,8]. These effects directly influence the fatigue strength of train structures, passenger aural comfort, and operational safety [9]. They also pose serious challenges to tunnel ancillary facilities, ventilation energy consumption during operation, and rescue and evacuation efficiency under emergency conditions [10,11]. By introducing regularly arranged openings in a perforated partition wall, limited airflow communication between both sides of the wall can be achieved. This allows active utilization of the train-induced piston effect to promote air exchange. In theory, this approach can

simultaneously mitigate pressure fluctuations, reduce aerodynamic drag, optimize ventilation performance, and facilitate emergency rescue. However, the introduction of a perforated partition wall substantially alters the evolution mechanisms of the three-dimensional, unsteady, compressible flow field inside tunnels. This leads to aerodynamic characteristics that are fundamentally different from those of conventional single-track or twin-tube tunnels. The double-track tunnel with a perforated partition wall is shown in Fig. 1. The rationality of the opening design parameters—including opening ratio, opening spacing, and opening distribution pattern—directly determines the effectiveness of aerodynamic mitigation. Therefore, systematically investigating the influence of perforated partition walls on the aerodynamic behavior of extra-long tunnels and optimizing their design parameters is of considerable theoretical significance and engineering value.

Figure 1: The Groene Hart double-track tunnel with a perforated partition wall.

Researchers worldwide have conducted extensive studies on tunnel aerodynamics and aerodynamic mitigation measures. With the advancement of computational fluid dynamics (CFD) and physical model testing techniques, research efforts have expanded toward the aerodynamic optimization of passive mitigation measures. These include ventilation shafts [12,13], cross passages [14], and tunnel entrance buffer structures [15,16]. In recent years, increasing attention has been devoted to perforated partition walls as a special structural configuration. The National Aerospace Laboratory of the Netherlands (NLR) explored tunnels equipped with perforated partition walls using compressed air cannon experiments [17]. Mei et al. [18], established analytical approaches for evaluating aerodynamic drag and pressure waves in tunnels with perforated partition walls. Their work was based on a one-dimensional unsteady compressible non-isentropic flow model and the method of characteristics employing generalized Riemann variables. They also investigated the influence of opening parameters on aerodynamic resistance, providing an important foundation for one-dimensional simulations. Further three-dimensional numerical simulation studies demonstrated that perforated partition walls can significantly balance the pressure between adjacent tunnel spaces through their “air-exchange effect” [19]. This effectively reduces the amplitude of pressure waves acting on both the train and tunnel surfaces [20]. These studies also clarified the effects of opening area and opening spacing. However, although three-dimensional numerical simulations are capable of capturing flow details with high fidelity, their computational cost is prohibitively high. This makes them unsuitable for multi-condition and full-parameter parametric analyses in extra-long tunnels. Consequently, comprehensive parametric studies and optimized design strategies remain insufficient. In particular, studies considering the coupled effects of opening ratio, opening spacing, and opening distribution patterns on the overall aerodynamic performance are still lacking [21–23].

Despite these advances, existing studies on perforated partition walls still have several limitations. First, most three-dimensional numerical simulations [19,20] are too computationally expensive for full-parameter optimization in extra-long tunnels. Their scope is therefore often limited to isolated parameter variations.

Second, previous one-dimensional models [18] are efficient but have not been systematically validated across a wide range of opening parameters. They have also rarely been applied to multi-parameter optimization. Third, the coupled effects of opening ratio, spacing, and layout on both sides of the partition wall remain underexplored. As a result, designers lack clear guidance on optimal configurations.

To address these gaps, this study develops and validates a one-dimensional model suitable for opening ratios up to 0.32. It systematically investigates the coupled effects of three key design parameters to identify optimal configurations for extra-long tunnels. The findings have direct implications for the design of perforated partition walls in extra-long tunnels (≥10 km) used in high-speed railways operating at 300 km/h or higher. By quantifying how opening parameters affect pressure wave mitigation, this work provides engineers with evidence-based design recommendations. These recommendations can help improve train operational safety, passenger comfort, and the durability of tunnel ancillary facilities. From a scientific perspective, this study establishes a validated one-dimensional modeling framework that enables efficient parametric optimization. This approach can be extended to other complex tunnel configurations.

2 Numerical Method

2.1 Physical Model and Governing Flow Equations

The basic physical model for airflow in the tunnel is shown in Fig. 2. When a high-speed train passes through a tunnel, it induces a complex airflow. This flow is three-dimensional, compressible, wave-dominated, and unsteady turbulent. Flow separation and three-dimensional unsteady turbulence of varying intensity occur near the train nose and tail. In general, the tunnel length is much larger than the hydraulic diameter of the tunnel cross-section. Pressure waves propagate inside the tunnel at approximately the speed of sound. After traveling a certain distance, the three-dimensional characteristics of the compression waves gradually diminish. The waves then evolve into one-dimensional plane waves [3]. Therefore, the three-dimensional flow within the tunnel can be simplified as a one-dimensional unsteady compressible flow. The three-dimensional unsteady turbulent flows near the train nose and tail are approximated using pressure loss coefficients.

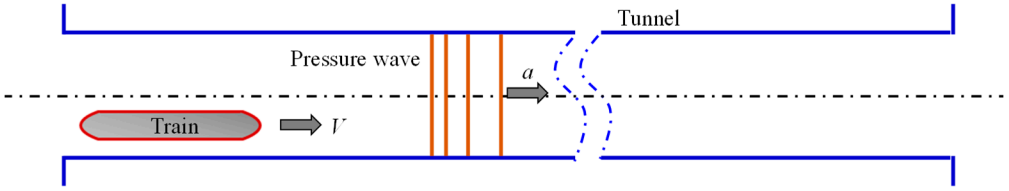

Figure 2: Basic physical model of tunnel airflow.

Considering that, in practical tunnels, friction and heat transfer occur between the air and both the tunnel walls and the train surfaces, the tunnel airflow can ultimately be simplified as a one-dimensional unsteady compressible non-isentropic flow [24].

Using the principles of mass, momentum, and energy conservation, the governing equations for the control volume are established. The term $\mathrm{d}F/\mathrm{d}x$ in Eq. (1) accounts for the cross-sectional area variation along the tunnel axis. For constant-area tunnel sections, this term vanishes, and the continuity equation reduces to its standard form. However, the general form is retained here to accommodate possible area changes at tunnel portals, buffer structures, or regions with openings. Detailed derivations can be found in Pope [25].

Continuity equation:

$$\frac{\partial \rho}{\partial t} + \rho \frac{\partial u}{\partial x} + u \frac{\partial \rho}{\partial x} + \rho \frac{u}{F} \frac{\mathrm{d}F}{\mathrm{d}x} = 0 \tag{1}$$

Momentum equation:

$$\frac{\partial u}{\partial t} + u \frac{\partial u}{\partial x} + \frac{1}{\rho} \frac{\partial p}{\partial x} + G = 0 \tag{2}$$

Energy equation:

$$\frac{\partial p}{\partial t} + u \frac{\partial p}{\partial x} + a^2 \left(\frac{\partial \rho}{\partial t} + u \frac{\partial \rho}{\partial x} \right) = (\kappa - 1)\rho(q - \xi + uG) \tag{3}$$

where u is the air velocity in the tunnel; p is the tunnel air pressure; κ is the specific heat ratio of air; ρ is the air density; a is the speed of sound in air; F is the cross-sectional area of the flow passage; G denotes the wall-friction term; q denotes the heat-transfer term between the air and the wall; ξ is the friction work associated with the train surface; and t is time. The tunnel airflow domain can be divided into the annular region formed between the train and the tunnel wall, and the tunnel region without a train. For these two flow regions, the specific expressions of the friction term G, the heat-transfer term q, and the train-surface friction work term ξ in the above equations are given as follows.

Annular region with a high-speed train.

$$G = \frac{1}{2F_{\mathrm{AN}}} [f_{\mathrm{TU}} u|u| S_{\mathrm{TU}} + f_{\mathrm{TR}} (u - V)|u - V| S_{\mathrm{TR}}] \tag{4}$$

$$q = \frac{1}{2F_{\mathrm{AN}}} \frac{\kappa R}{\kappa - 1} [f_{\mathrm{TR}} S_{\mathrm{TR}} |u| (T_{\mathrm{TR}} - T) + f_{\mathrm{TR}} S_{\mathrm{TR}} |u - V| (T_{\mathrm{TR}} - T)] \tag{5}$$

$$\xi = \frac{S_{\mathrm{TR}}}{2F_{\mathrm{AN}}} f_{\mathrm{TR}} V(u - V)|u - V| \tag{6}$$

where $F_{\mathrm{AN}} = F_{\mathrm{TU}} - F_{\mathrm{TR}}$, F_{TR}, S_{TR}, f_{TR} and V denote the train cross-sectional area, train perimeter, train surface friction coefficient, and train speed, respectively; T_{TR} is the train surface temperature.

Tunnel region without a train.

$$G = \frac{1}{2F_{\mathrm{TU}}} f_{\mathrm{TU}} u|u| S_{\mathrm{TU}} \tag{7}$$

$$q = \frac{1}{2F_{\mathrm{TU}}} \frac{\kappa R}{\kappa - 1} f_{\mathrm{TU}} S_{\mathrm{TU}} |u| (T_{\mathrm{TU}} - T) \tag{8}$$

$$\xi = 0 \tag{9}$$

where S_{TU} is the tunnel cross-sectional perimeter; F_{TU} is the tunnel cross-sectional area; f_{TU} is the tunnel wall friction coefficient; T_{TU} is the tunnel wall temperature; and T is the tunnel air temperature.

Fig. 3 illustrates the geometry of a tunnel with a perforated partition wall. When a high-speed train passes through a tunnel equipped with a built-in perforated partition wall, the physical model of the

airflow differs from that of a tunnel without a partition wall. However, the basic form of the governing equations remains unchanged. The tunnel spaces on the two sides of the partition wall can be treated as two independent tunnel sections. Airflow exchange between these sections occurs through the openings. Fig. 4 shows the airflow physics model for a tunnel containing an internal perforated partition wall. In each tunnel space, the streamwise flow effects along the tunnel axis are much more pronounced than the radial flow effects. Therefore, radial flow can be neglected. Accordingly, the airflow in each tunnel space separated by the perforated partition wall is modeled as a one-dimensional flow. When the train travels in one of the tunnel spaces, the ground effect associated with train motion is assumed to be negligible. The train passage process is simplified as the motion of a cylindrical train within a coaxial cylindrical tunnel. In contrast, the airflow in the other tunnel space is influenced only by the mass transfer through the openings in the perforated partition wall.

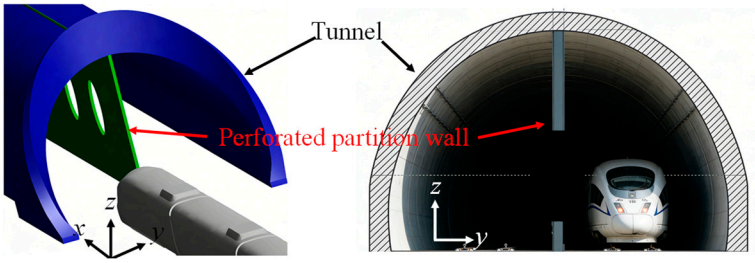

Figure 3: Geometric model of a tunnel with a perforated partition wall.

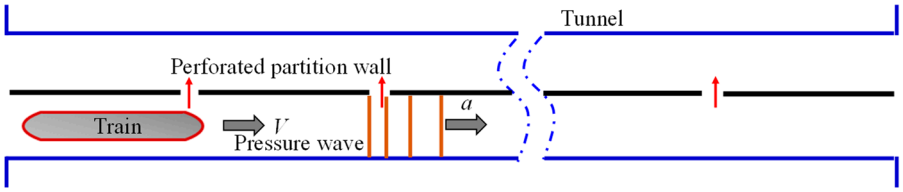

Figure 4: Tunnel airflow physics model with a built-in perforated partition wall.

The thin-plate (sharp-edged) orifice model is adopted to derive the flow-rate equation for the openings in the perforated partition wall. This model is based on the orifice-discharge assumption. It is further assumed that the airflow through an opening is parallel to the orifice centerline. Under these assumptions, the volumetric flow rate through the orifice is expressed as:

$$q_{\mathrm{v}} = A_{\mathrm{c}} v_{\mathrm{c}} = C_{\mathrm{c}} A v_{\mathrm{c}} = C_{\mathrm{c}} C_{\mathrm{v}} A \sqrt{\frac{2\Delta p}{\rho}} \tag{10}$$

where $C_{\mathrm{q}} = C_{\mathrm{c}} C_{\mathrm{v}} = \frac{C_{\mathrm{c}}}{\sqrt{1+\xi}}$ is the orifice discharge coefficient. Since the airflow through the partition openings satisfies the sharp-edged thin-wall orifice condition, the flow rate through a partition-wall opening can be written as:

$$q_{\mathrm{m}} = \alpha F \sqrt{2\rho g |\Delta p|} \tag{11}$$

where α is the discharge coefficient of the opening. As the Reynolds number of the gas flow is generally above 10^5, α is taken as 0.62 in the numerical implementation; F is the opening area. By incorporating the above orifice flow-rate relations into the one-dimensional tunnel airflow model without a partition wall, a

one-dimensional tunnel airflow model with a built-in perforated partition wall can be obtained. The units of the variables used in the equations in this section are listed in the following Table 1.

Table 1: Units of variables used in the governing equations.

Symbol	Meaning	Unit
ρ	Density	kg/m^3
a	Speed of sound	m/s
t	Time	s
u	Airflow velocity	m/s
p	Pressure	Pa
F	Area	m^2
S	Perimeter	m
G	Friction term	N
q	Heat transfer term per unit time	W
ξ	Frictional work per unit time	W
T	Temperature	K

2.2 Grid Discretization and Numerical Solution Method

The governing equations of the one-dimensional unsteady compressible non-isentropic flow adopted in this study form a first-order quasi-linear hyperbolic system of partial differential equations. Therefore, the method of characteristics is employed to solve them [2]. Two approaches can be used within the framework of the method of characteristics. The first approach directly solves the characteristic equations expressed in terms of primitive flow variables, such as velocity, pressure, and density. This is referred to as the primitive-variable characteristic method. The second approach transforms the characteristic equations into a form expressed in terms of Riemann variables. After solving the resulting characteristic equations, the target flow parameters—including velocity and pressure—are obtained through the relationships between the Riemann variables and the primitive variables. This approach is known as the generalized Riemann variable characteristic method. The generalized Riemann variable characteristic method can be further classified into dimensional and nondimensional formulations. In this study, the nondimensional generalized Riemann variable characteristic method is adopted.

The grid system for a train passing through a tunnel with a built-in perforated partition wall is established separately for tunnel sections with and without a train. This study investigates the entire process of a train passing through a tunnel. From a spatial perspective, this process can be divided into three regions: the space ahead of the train, the space currently occupied by the train (annular space), and the space behind the train. Based on the variation of grid spacing over time, the grids are classified into three types: compressed grids, stretched grids, and fixed-length grids. As shown in Fig. 5, the region ahead of the train corresponds to nodes 1 to i + 1, where the grid cell (i, i + 1) is a boundary cell. As the nose tip moves forward, the distance between points i + 1 and i continuously decreases. When the nose tip passes point i, the grid cell (i, i + 1) disappears, and the cell (i − 1, i) becomes the next cell whose length decreases over time. Such grids, whose length decreases with time, are called compressed grids. Similarly, the region behind the train corresponds to nodes 1 to k + 1, where the grid cell (k, k + 1) is a boundary cell. As the rear nose tip moves forward, the distance between points k and k + 1 continuously increases. When this distance reaches a full grid length, a new grid cell (k + 1, k + 2) is formed. Consequently, the cell (k − 1, k) becomes one whose length increases over time. Such grids, whose length increases with time, are called stretched grids. The grids formed by nodes 1 to i and 1 to k maintain a constant length throughout the calculation. These are referred to as fixed-length grids.

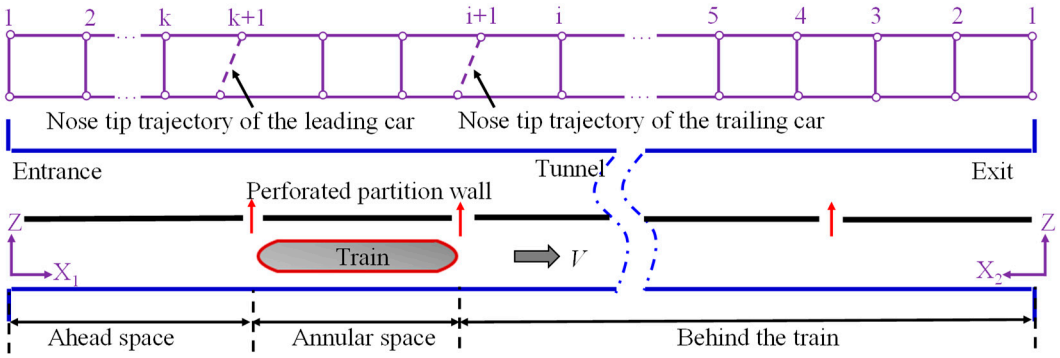

Figure 5: Schematic of the mesh system during train operation inside the tunnel.

Fig. 6 shows the mesh system for a train running inside a tunnel. The tunnel region without a train can be treated as a duct flow with openings. Its grid system consists of uniform fixed-length cells defined in a ground-fixed reference frame. The grid system for the tunnel section with a train is identical to that used for a train passing through a tunnel without a partition wall. The regions ahead of and behind the train are discretized using compressed grids, stretched grids, and fixed-length grids, respectively. The annular region formed by the tunnel and the train is discretized using fixed-length grids defined in a train-fixed reference frame.

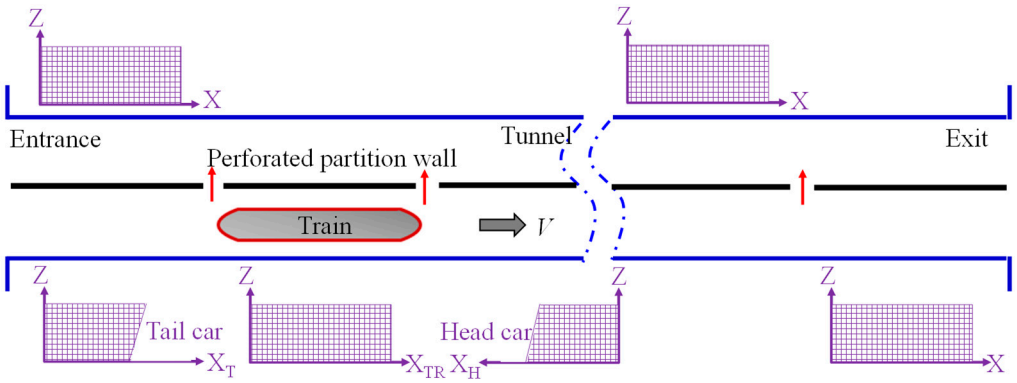

Figure 6: Moving mesh system for a train in a tunnel.

2.3 Validation of the Numerical Method

In this study, a one-dimensional flow calculation method is employed to predict the pressure waves in the Dordtsche Kil tunnel equipped with a perforated partition wall. The results are compared with the experimental data and numerical results reported in Ref. [17]. This comparison verifies the validity of the proposed one-dimensional flow model for simulating pressure fluctuations in tunnels with built-in perforated partition walls. The detailed computational parameters are listed in Table 2.

Table 2: Numerical validation parameters for pressure waves.

	Length/m	Cross-Sectional Area/m^2	Opening Diameter/m	Opening Spacing/m	Speed/(km·h^{-1})
Tunnel	1330	50	0.72	25	/
Train	400	9.45	/	/	300

Fig. 7 presents comparisons of pressure fluctuations measured at a ground monitoring point located 500 m from the tunnel entrance. Measurements were taken on both the train-passing side and the non-train side. The comparison includes experimental data [17] numerical results from the literature, and the results obtained in this study for the case with a perforated partition wall. As shown in the Fig. 7, the pressure fluctuation curves predicted by the present model agree well with the experimental results reported in the literature. They exhibit nearly identical attenuation trends and accurately capture each pressure peak. On the train-passing side, the relative errors of the predicted positive and negative pressure peaks with respect to the experimental data are −4.2% and −4.0%, respectively. On the non-train side, the agreement is also satisfactory, with relative errors within 10% for both peak values. These results demonstrate that the proposed one-dimensional calculation method can accurately predict the pressure fluctuation characteristics in tunnels with built-in perforated partition walls.

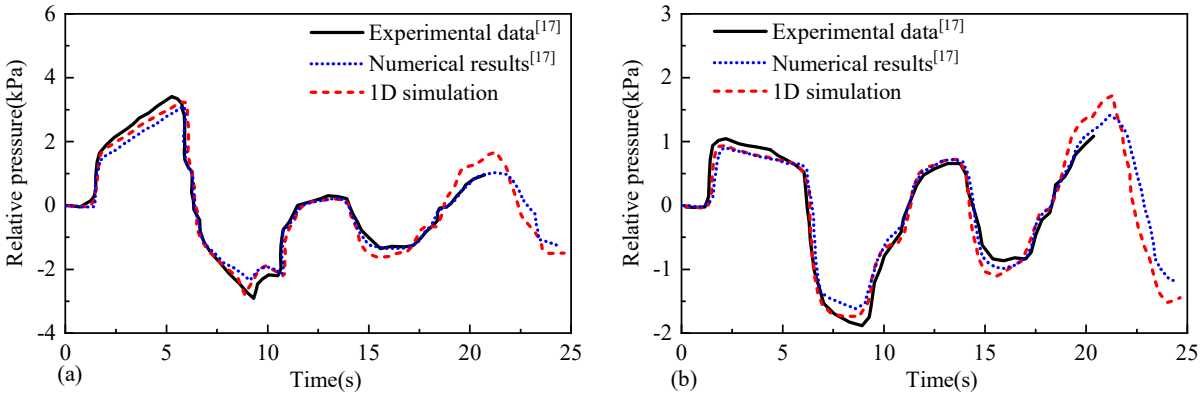

Figure 7: Pressure fluctuation curves at 500 m into the entrance of the tunnel in a double-track tunnel with a partition during single-train passage: (**a**) The train-passing side, (**b**) The non-train side. Experimental data and numerical results are from [17].

To further demonstrate the accuracy of the proposed one-dimensional method in the absence of full-scale test data for a CRH2 train in a perforated-partition tunnel, this study follows the research approach of Linic et al. [26]. A validation case is considered involving a single CRH2 train in a four-car formation passing through a 1000 m tunnel equipped with a perforated partition wall with an opening ratio of 0.13. As shown in Fig. 8, the results obtained using the one-dimensional method are compared with those from three-dimensional numerical simulations.

In this study, the opening ratio of the partition wall is defined as the ratio of the perimeter of a single opening to the wetted perimeter of the tunnel on the train-passing side. This definition is adopted because, in one-dimensional flow modeling, the mass exchange through openings is governed by the perimeter length rather than the area. The flow through thin-plate orifices is primarily influenced by the edge length. This differs from the conventional engineering definition of opening ratio as the ratio of open area to total wall area, which is more relevant for structural design and visual permeability assessments. Fig. 8 presents a comparison between the three-dimensional numerical simulation results and those obtained using the one-dimensional calculation method. As shown in the figure, the pressure fluctuation curves predicted by the proposed one-dimensional method exhibit good agreement with the three-dimensional simulation results. The maximum relative error is on the order of 10%. This demonstrates that the one-dimensional approach can accurately capture the pressure fluctuation characteristics on both sides of the partition wall within the tunnel.

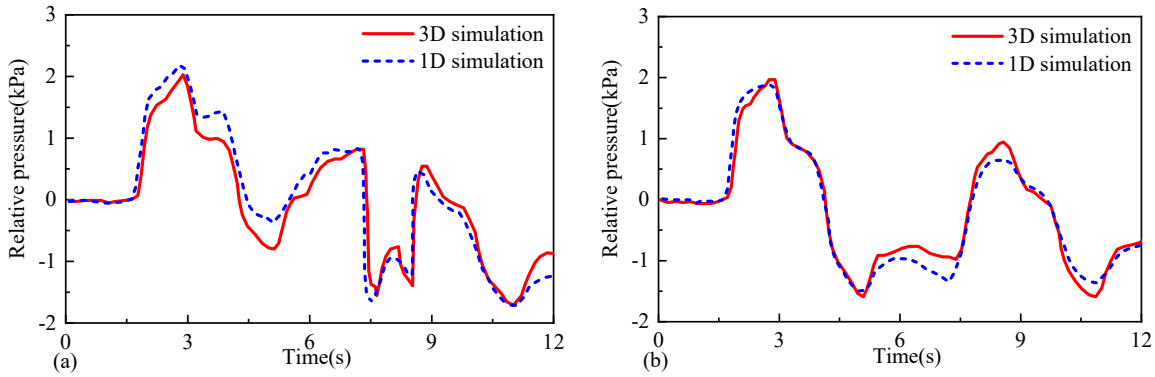

Figure 8: Simulation results comparison of pressure waves for a single train passing through a tunnel with a perforated partition wall: (**a**) The train-passing side, (**b**) The non-train side.

While direct experimental validation for the CRH2 train in a 10 km tunnel with a perforated partition wall is not feasible within this study, the one-dimensional model is validated against two independent datasets. The first dataset comes from model-scale experiments on the Dordtsche Kil tunnel. The second dataset is obtained from three-dimensional CFD simulations for the CRH2 train in a 1000 m tunnel with a perforated wall, as shown in Fig. 8. The good agreement with both datasets provides confidence in the model's predictive capability for the full-scale CRH2 case. Future work should include field measurements on operational high-speed lines to further validate the numerical predictions.

2.4 Applicability Range

Fig. 9 illustrates the pressure fluctuation curves on the train-passing side during the passage of a CRH2G train traveling at 300 km/h through a tunnel equipped with a built-in perforated partition wall. For a double-track tunnel with a cross-sectional area of 100 m^2, when the opening ratio of the partition wall is 0.20 or lower, the pressure–time histories obtained from the one-dimensional calculations are smooth and free from abnormal oscillations. When the opening ratio increases to 0.32, the overall trend of the pressure–time curve remains unchanged. However, small-amplitude oscillations begin to appear. At an opening ratio of 0.45, the one-dimensional calculation can still reflect the general trend of pressure fluctuations, but the oscillations become significantly more pronounced. When the opening ratio further increases to 0.55, the pressure–time history predicted by the one-dimensional model exhibits severe oscillations. It can no longer represent the underlying pressure-wave propagation characteristics. Based on these observations, the one-dimensional flow model established in this study is applicable to cases with partition-wall opening ratios not exceeding 0.32.

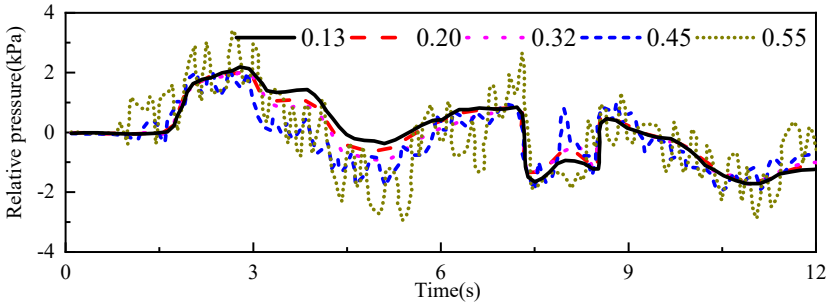

Figure 9: One-dimensional numerical simulation results of pressure in the tunnel under different opening ratios.

The threshold of 0.32 is therefore not arbitrary. It corresponds to the onset of significant nonlinear interactions between openings and the breakdown of the plane-wave assumption. At low opening ratios, the flow through openings behaves as sharp-edged orifice flow with a stable discharge coefficient. As the opening ratio increases beyond 0.32, adjacent openings begin to interact aerodynamically. This interaction alters the local pressure distribution and causes the effective discharge coefficient to deviate from the thin-plate assumption. Consequently, inaccuracies arise in the modeled mass exchange rate. In addition, wave propagation distortion occurs. In the one-dimensional model, pressure waves are assumed to propagate as plane waves. When openings become sufficiently large or numerous, the wave fronts become distorted due to three-dimensional effects near the openings. As a result, the one-dimensional approximation breaks down. This breakdown manifests as numerical oscillations in the pressure-time histories, as shown in Fig. 9. These oscillations indicate that the model no longer accurately captures the underlying physics.

3 Results and Discussion

This study takes an eight-car CRH2 electric multiple unit (EMU) traveling at 300 km/h through a 10 km extra-long tunnel as the research object. The tunnel has a clear cross-sectional area of 100 m^2. The aim is to investigate the influence of built-in partition walls on tunnel aerodynamic effects and to propose an optimized partition wall design scheme for extra-long tunnels. This study focuses on circular openings with a diameter of 0.72 m, as used in the validated Dordtsche Kil tunnel case. The effect of opening shape—such as rectangular, slotted, or elliptical configurations—on discharge coefficients and pressure wave attenuation has not been investigated. Different shapes with the same area may exhibit different local flow resistance due to variations in vena contracta formation and edge effects. For example, sharp-edged rectangular openings typically have slightly lower discharge coefficients than circular ones, which could affect air-exchange efficiency.

3.1 Effect of the Partition Wall on Tunnel Pressure Waves

Figs. 10 and 11 compare the pressure fluctuation curves for three tunnel configurations: a tunnel without a partition wall, a tunnel with a solid (non-perforated) partition wall, and a tunnel with a perforated partition wall. The comparisons are made at the central monitoring point of the double-track tunnel and at points on the train. For the perforated partition wall case, a uniformly distributed opening arrangement along the entire wall is adopted, with an opening area of 2 m^2 and an opening spacing of 10 m. As shown in the Figs. 10 and 11, the solid partition wall completely isolates the two tunnels, resulting in no pressure fluctuations at the midpoint of the non-train side tunnel. Apart from this, the pressure fluctuation trends in the train-side tunnel are consistent across all three configurations. Only the peak values differ. The solid partition wall isolates the non-train side tunnel but reduces the effective airflow area in the train-side tunnel. This leads to a sharp increase in pressure within the tunnel. Compared to the configuration without a partition wall, the maximum positive and negative pressure values increase by 149% and 137%, respectively. The maximum positive pressure at the train nose tip increases by 239%, and the maximum negative pressure at the train tail increases by 136%. These increases pose a safety risk to train operation. After uniform openings are introduced into the partition wall, the amplitude of pressure fluctuations in the tunnel becomes similar to that in the configuration without a partition wall. However, in the perforated partition wall case, the maximum positive and negative pressure values on the non-train side increase by 17.7% and 11.4%, respectively, compared to the configuration without a partition wall.

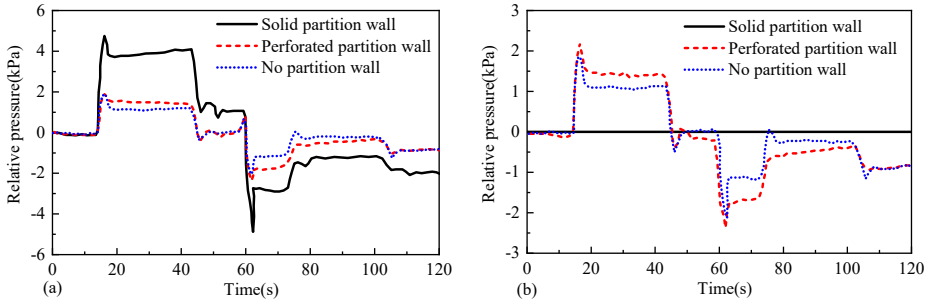

Figure 10: Influence comparison of a perforated partition wall on pressure fluctuations in a tunnel: (**a**) The train-passing side, (**b**) The non-train side.

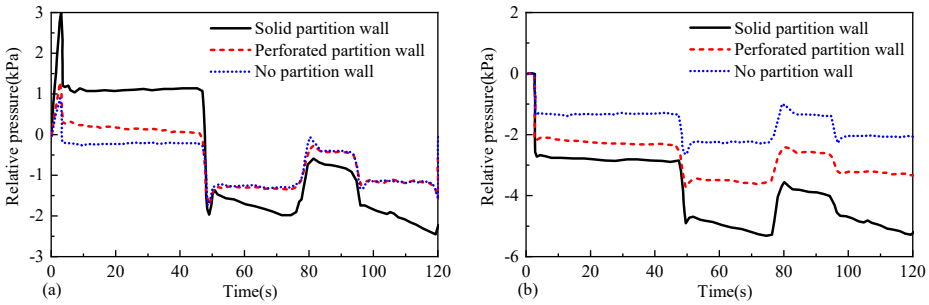

Figure 11: Influence comparison of a perforated partition wall on pressure fluctuations in a tunnel: (**a**) Leading car, (**b**) Trailing car.

Fig. 12 shows the pressure fluctuation amplitudes and the corresponding reduction ratios at the central monitoring point of the tunnel and on the exterior of the train on the train-passing side under different partition wall configurations. When a solid (non-perforated) partition wall is installed, the blockage ratio doubles. This causes a significant increase in pressure fluctuation amplitudes both inside the tunnel and outside the train. In this case, the peak-to-peak pressure fluctuation within the tunnel is approximately twice that observed for the other two configurations. Compared with the solid partition wall configuration, the uniformly distributed perforated partition wall scheme and the configuration without a partition wall reduce the pressure variation amplitudes at the tunnel central monitoring point and at the train nose exterior by approximately 41.7% and 41.4%, respectively. In addition, the maximum pressure variation amplitude at the train tail exterior is reduced by approximately 28.5% relative to the solid partition wall configuration.

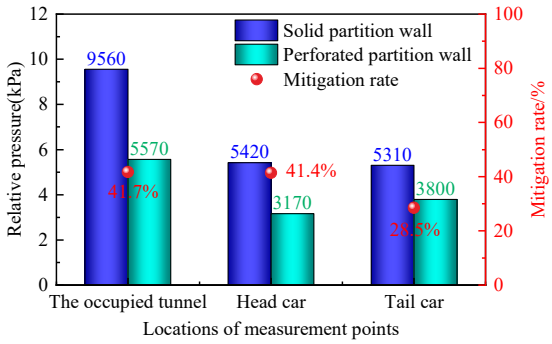

Figure 12: Mitigation effect of a perforated partition wall on pressure fluctuations.

3.2 Effect of Partition Wall Opening Ratio

Fig. 13 presents the pressure–time histories at the central monitoring points of the train-passing side and the non-train side of the tunnel for different opening ratios. The train travels at 300 km/h through a tunnel equipped with a perforated partition wall with an opening spacing of 10 m. As shown in the Fig. 13, at the central location of the 10 km tunnel, the pressure fluctuation characteristics on both sides of the partition wall are only weakly influenced by the opening area. Noticeable differences associated with the opening ratio appear only locally before the train passes the monitoring point. In these local regions, larger opening ratios result in more intense pressure variations.

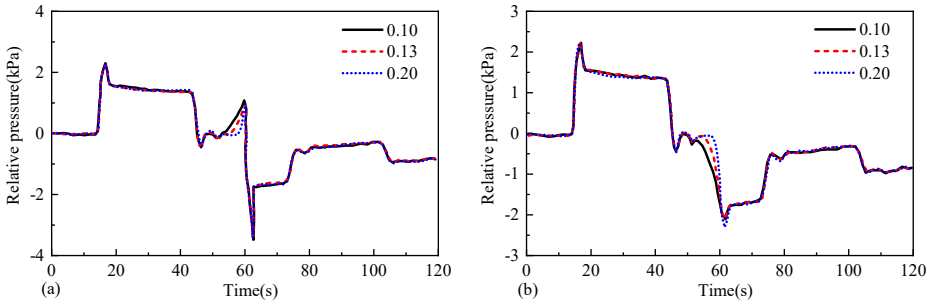

Figure 13: Effect of the partition wall opening ratio on the tunnel pressure wave: (**a**) The train-passing side, (**b**) The non-train side.

Fig. 14 shows the maximum positive and negative pressures, as well as the peak-to-peak pressure amplitudes, at the central monitoring point on both the train-passing side and the non-train side of the tunnel for partition walls with different opening ratios. As the opening area increases, the airflow between the two tunnel spaces on either side of the partition wall intensifies. Consequently, the peak-to-peak pressure within the tunnel on the train-passing side gradually decreases. Compared with the opening ratio of 0.1, the peak-to-peak pressure decreases by 2.4% when the opening ratio reaches 0.2. Conversely, the amplitude of pressure fluctuations on the non-train side increases. The peak-to-peak value rises from 4300 Pa to 4600 Pa, representing an increase of 7.0%. During the train passage process, increasing the opening ratio enhances air exchange between the tunnel spaces on both sides of the partition wall. This leads to smaller pressure fluctuations on the train-passing side, which is beneficial for train operational safety.

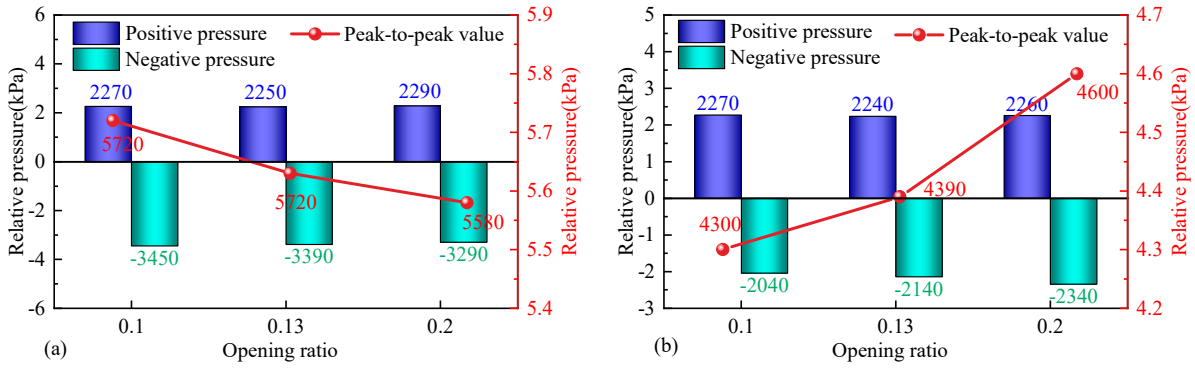

Figure 14: Effect of the partition wall opening ratio on the amplitude of pressure variation at the central measuring point inside the tunnel: (**a**) The train-passing side, (**b**) The non-train side.

Increasing the opening ratio means a larger total opening area per unit length of the partition wall. This enhances airflow exchange between the two sides of the tunnel. According to orifice flow theory, the flow velocity through an opening is proportional to the square root of the pressure difference. Therefore, under the same pressure difference, a larger opening area allows more airflow exchange. Pressure waves on the train-passing side can be partially released to the non-train side through the openings. This reduces the amplitude of pressure fluctuations on the train-passing side. At the same time, more airflow enters the non-train side, disturbing the originally still air and inducing pressure fluctuations there. The amplitude of pressure fluctuations on the non-train side (<400 Pa) is well below the design load of tunnel ancillary structures. It poses no safety risk to these facilities. However, long-term fatigue effects warrant further investigation.

3.3 Effect of Opening Spacing in the Partition Wall

Fig. 15 illustrates the influence of opening spacing on the pressure variation trends at the central monitoring point of the tunnel. The train travels at 300 km/h through a tunnel equipped with a uniformly perforated partition wall with an opening ratio of 0.20. As shown in the Fig. 15, the pressure fluctuation patterns on the train-passing side remain largely consistent across different opening spacings. Differences in pressure amplitude do not exceed 10%. For a fixed total opening area, increasing the opening spacing reduces the number of openings available for air exchange between the two tunnel spaces. This weakens the mass transfer through the openings. Consequently, pressure fluctuations on the train-passing side become more intense. The maximum positive pressure, maximum negative pressure, and peak-to-peak pressure amplitude all increase. In contrast, pressure fluctuations on the non-train side generally become more subdued.

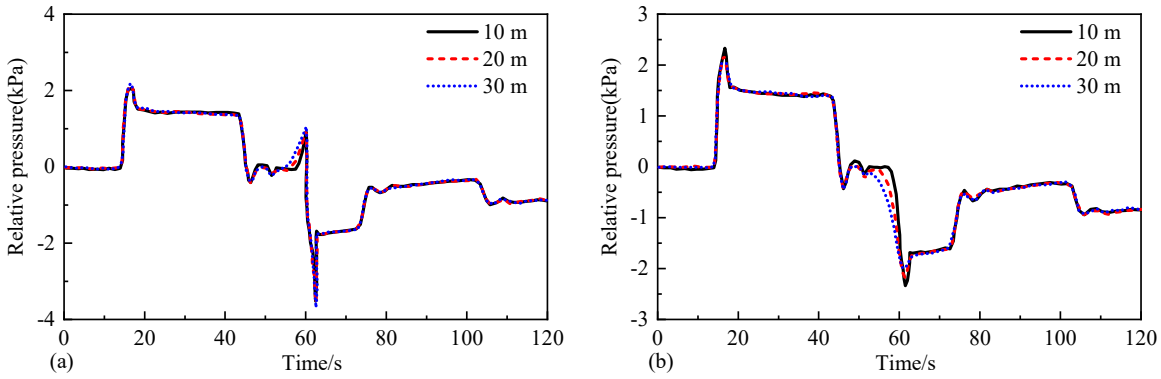

Figure 15: Effect of opening spacing in the partition wall on the tunnel pressure wave: (**a**) The train-passing side, (**b**) The non-train side.

Figs. 16 and 17 show the maximum positive pressure, maximum negative pressure, and peak-to-peak pressure outside the leading car and the trailing car during the train's passage through the tunnel. As shown in the Figs. 16 and 17, under fixed opening location and opening ratio conditions, increasing the opening spacing weakens the air exchange between the two tunnel spaces separated by the partition wall. As a result, the amplitude of pressure fluctuations outside both the leading and trailing cars increases significantly. When the opening spacing is 10 m, the maximum positive pressure outside the leading car is 1460 Pa. As the opening spacing increases to 30 m, the maximum positive pressure rises to 1700 Pa. This represents a growth rate of 16.4%. When the opening spacing increases from 10 m to 30 m, the maximum negative pressure outside the trailing car increases from −4000 Pa to −4080 Pa, a growth rate of 2%. These

results indicate that increasing the opening spacing has a greater impact on the operational safety of the leading car than on the trailing car.

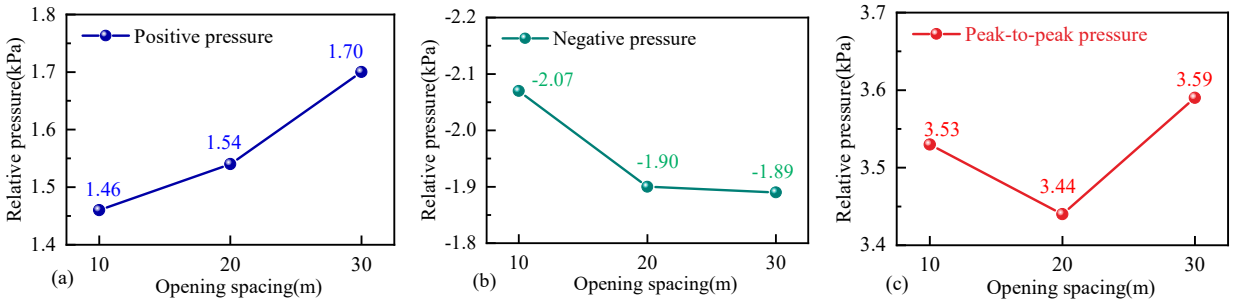

Figure 16: Effect of opening spacing on the pressure fluctuation amplitude around the leading car: (**a**) The maximum positive pressure, (**b**) The maximum negative pressure, (**c**) Peak-to-peak pressure.

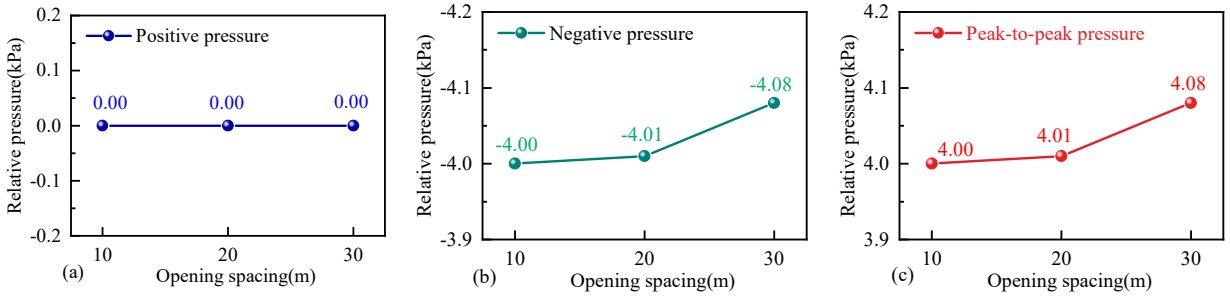

Figure 17: Effect of opening spacing on the pressure fluctuation amplitude around the trailing car: (**a**) The maximum positive pressure, (**b**) The maximum negative pressure, (**c**) Peak-to-peak pressure.

3.4 Effect of Opening Location in the Partition Wall

Based on the preceding analysis, for a 10 km tunnel equipped with a built-in perforated partition wall and under the three opening ratios investigated, increasing the opening area and reducing the opening spacing is favorable for mitigating pressure fluctuations outside the train. Accordingly, an opening ratio of 0.20 combined with an opening spacing of 10 m is identified as the optimal opening configuration. On this basis, this section further investigates the influence of opening location on tunnel pressure fluctuations. Pressure variations on both the train-passing side and the non-train side of the tunnel are compared under different opening arrangement schemes. To ensure a fair comparison, the total number of openings is kept approximately the same by adjusting the opening spacing. Three perforation configurations are shown in Fig. 18. For the uniformly distributed opening scheme along the entire tunnel length, openings are arranged at intervals of 20 m, resulting in a total of 499 openings. For the other schemes, openings are arranged at a spacing of 10 m. In the central opening scheme, 499 openings are distributed around the tunnel midpoint. In the end-opening scheme, 250 openings are installed near the tunnel entrance and 250 near the tunnel exit, yielding a total of 500 openings.

Fig. 19 presents the pressure fluctuation curves within the tunnels on both sides of the partition wall for the three opening arrangement schemes described above. As shown in the Fig. 19, the pressure fluctuation trends at the central monitoring points are generally similar across the different opening location scenarios. However, notable differences appear in the local peak values. In the uniform opening scheme and the central opening scheme, the central monitoring points are located within the perforated sections of the

partition wall. As a result, their pressure fluctuation curves nearly overlap, with differences in pressure amplitude remaining within 5%. In the end-opening scheme, the central section containing the monitoring points has no openings. The enclosed space formed by the tunnel wall and the partition wall restricts the airflow, leading to more intense pressure fluctuations compared to the other two schemes. Specifically, relative to the central opening scheme, the maximum positive pressure on the train-passing side increases by 83%, and the maximum negative pressure increases by 53%. In the end-opening scheme, the pressure curves on the non-train side are more complex. However, compared to the other schemes, the differences in both the maximum positive and negative pressure values are less than 10%.

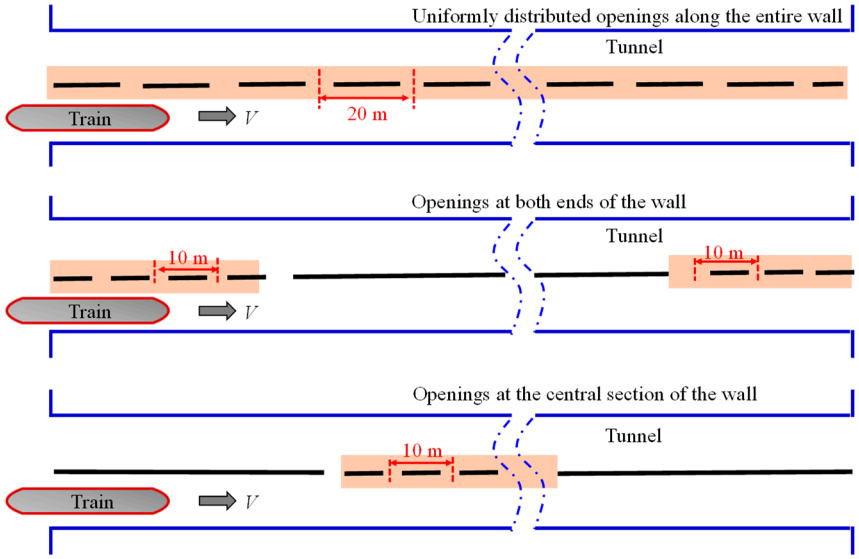

Figure 18: Schematic of different opening locations.

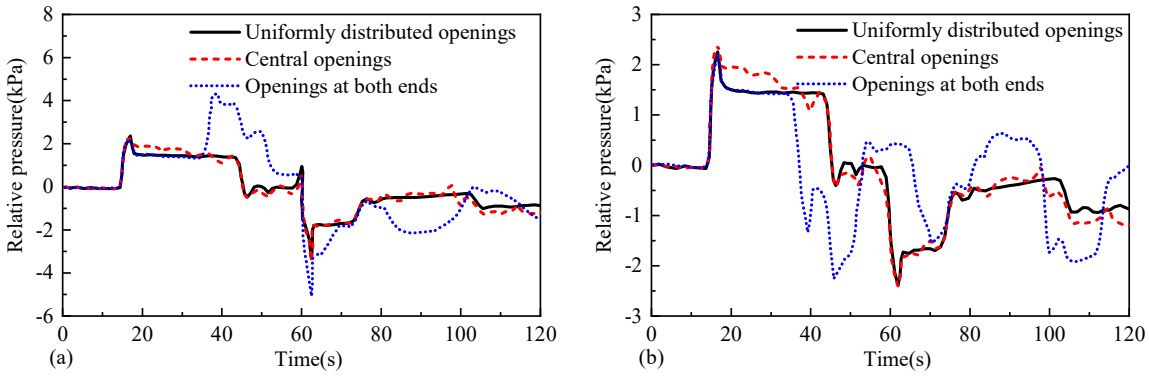

Figure 19: Effect of opening location in the partition wall on the pressure wave inside the tunnel: (**a**) The train-passing side, (**b**) The non-train side.

Fig. 20 illustrates the exterior pressure fluctuation curves of the leading car and the trailing car as the train passes through the tunnel under the three opening location schemes described above. As shown in the Fig. 20, the pressure fluctuations outside both the leading and trailing cars are the smoothest under the uniform opening scheme. In the end-opening and central opening schemes, the pressure outside the leading car exhibits significant fluctuations around 30 s and 90 s, respectively. Such fluctuations may affect the operational stability of the train inside the tunnel. Both the end-opening and uniform opening schemes

effectively relieve pressure as the train enters the tunnel, mitigating the intensity of the compression wave ahead of the train. In contrast, under the central opening scheme, the train passes through an unperforated section of the partition wall upon entry. Consequently, the initial pressure amplitude outside the leading car is significantly higher than in the other two schemes. Specifically, compared to the uniform opening scheme, the maximum positive pressure outside the leading car increases by 86%. Compared to the end-opening scheme, it increases by 133%. Under the end-opening scheme, as the trailing car passes through the tunnel, the expansion wave sweeps over the train tail precisely when the train is located in an unperforated section. At this moment, pressure fluctuations cannot be effectively relieved. This results in a significantly larger pressure amplitude at the trailing car compared to the other schemes. The maximum negative pressure outside the trailing car increases by 49.7% relative to the uniform opening scheme. Overall, the uniform opening scheme exhibits the smoothest pressure fluctuations outside both the leading and trailing cars, along with smaller maximum pressure amplitudes. This is advantageous for ensuring the safety of train operations inside the tunnel.

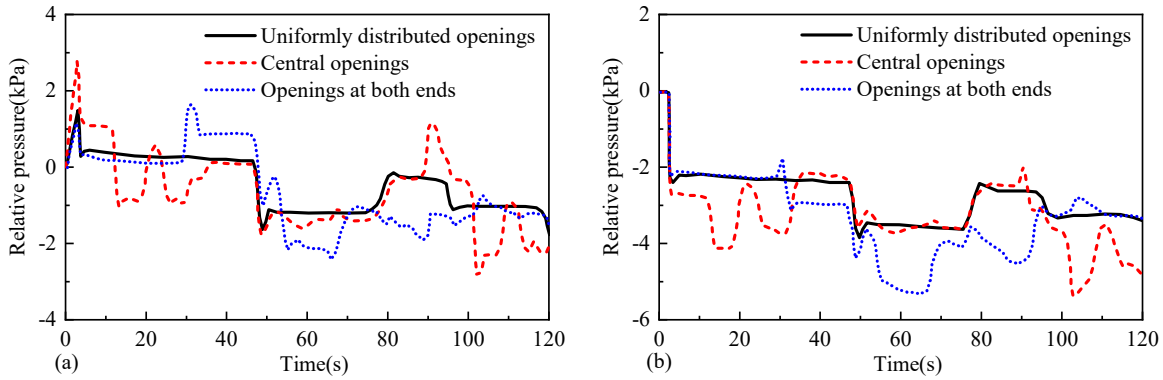

Figure 20: Effect of opening location in the partition wall on pressure fluctuations around the train: (**a**) Leading car, (**b**) Trailing car.

While the uniformly distributed opening scheme with a ratio of 0.20 and a spacing of 10 m yields the best aerodynamic performance, its engineering feasibility requires discussion. Installing approximately 1000 openings along the partition wall of a 10 km tunnel involves significant construction cost and maintenance complexity. Each opening requires edge reinforcement to prevent stress concentration and fatigue cracking under cyclic pressure loading. The structural integrity of the perforated wall under long-term train-induced vibrations and potential seismic loads would also need careful evaluation.

4 Conclusion and Outlook

This study employs a one-dimensional flow model to systematically investigate the aerodynamic effects of built-in partition walls in extra-long tunnels. A multi-factor analysis is conducted considering opening ratio, opening spacing, and opening location. Based on this analysis, an optimized partition wall design scheme for extra-long tunnels is proposed. The practical significance of this work lies in providing quantitative design guidelines for perforated partition walls. These guidelines enable engineers to select appropriate opening parameters that optimally balance pressure mitigation on both sides of the partition. From a scientific perspective, the main contribution is the development and validation of a one-dimensional modeling approach. This approach captures the essential physics of airflow exchange through openings while maintaining computational efficiency for extra-long tunnels. The main conclusions are as follows:

(1) Based on orifice flow theory, this study develops a one-dimensional unsteady compressible flow model for tunnels with built-in perforated partition walls. The model is validated against both model-scale experiments on the Dordtsche Kil tunnel and three-dimensional CFD simulations. It accurately captures train-induced pressure fluctuations for opening ratios up to 0.32 while being computationally efficient for extra-long tunnels. This provides a practical tool for multi-parameter optimization where full 3D simulations are infeasible.

(2) Compared with a solid partition wall, a uniformly distributed perforated wall with an opening ratio of 0.20 and a spacing of 10 m reduces pressure fluctuation amplitudes inside the tunnel by 41.7%. The peak positive pressure outside the leading car decreases by 41.4%, and the peak negative pressure outside the trailing car decreases by 28.5%. These quantitative results provide direct design guidance for aerodynamic mitigation measures in tunnels.

(3) Increasing the opening ratio or decreasing the opening spacing enhances airflow exchange between the two tunnel spaces separated by the partition wall. Pressure waves on the train-passing side are partially released to the non-train side through the openings, thereby reducing pressure fluctuations on the train-passing side. Meanwhile, airflow entering the non-train side induces pressure fluctuations there, though their amplitude (<400 Pa) remains below the design load of tunnel ancillary structures. This mechanistic understanding deepens the knowledge of perforated wall aerodynamics.

(4) Through systematic comparison of opening ratios (0.1, 0.13, 0.2), opening spacings (10 m, 20 m, 30 m), and opening layouts (uniform, central-concentrated, end-concentrated), the uniformly distributed layout with an opening ratio of 0.20 and a spacing of 10 m yields the best aerodynamic performance. This configuration produces the smoothest pressure fluctuations throughout the train passage, which is favorable for train operational safety.

(5) While the uniformly distributed scheme with 0.20 opening ratio and 10 m spacing is aerodynamically optimal, installing approximately 1000 openings along a 10 km tunnel involves significant construction cost and maintenance complexity. Each opening requires edge reinforcement to prevent fatigue cracking under cyclic loading. In practice, slightly modified schemes—such as a 0.15 opening ratio or 15 m spacing—may achieve acceptable aerodynamic performance with fewer openings, offering a practical compromise between performance and cost.

Future research should extend this work by investigating the influence of opening shape on aerodynamic performance. Variations in perimeter for a given opening area may alter mass exchange rates and pressure wave attenuation. Additionally, while the present analysis focuses on single-train passage at 300 km/h, further studies are needed to examine train encountering scenarios, variable speed profiles, and the effects of tunnel roughness and non-stationary wind environments. Work on two-train encountering scenarios is already underway, and future studies will also consider a wider range of operating conditions, including various tunnel lengths, train speeds, and opening schemes, to further advance the understanding of this problem. Finally, the optimal scheme proposed herein is based solely on aerodynamic performance. Future work should integrate structural integrity, construction cost, maintenance requirements, and ventilation energy consumption to achieve truly optimal engineering solutions.

Acknowledgement: None.

Funding Statement: This work was supported by the Key Project of the China State Railway Group Co., Ltd. Science and Technology Research and Development Program (Grant No. N2020G040), the Science and Technology Research and Development Program of China Railway Group Limited (Grant CYD2025-Major Science and Technology

Projects-03) and the Science and Technology Research and Development Program of China Railway Group Limited (Grant No. kyy2025-Major Science and Technology Projects-01).

Author Contributions: The authors confirm contribution to the paper as follows: study conception and design: Yunchao Du, Xianming Shi; data collection: Zhiqiang Liu; analysis and interpretation of results: Yunchao Du, Jian Wu; draft manuscript preparation: Yunchao Du. All authors reviewed and approved the final version of the manuscript.

Availability of Data and Materials: The data presented in this study is available from the corresponding author, upon reasonable request. The data is not publicly available due to privacy.

Ethics Approval: Not applicable.

Conflicts of Interest: The authors declare no conflicts of interest.

Nomenclature

Symbols	Meaning	Unit
ρ	Air density inside the tunnel	kg/m^3
a	Speed of sound	m/s
t	Time	s
u	Airflow velocity inside the tunnel	m/s
V	Train speed	m/s
p	Pressure	Pa
F	Area	m^2
S	Perimeter	m
G	Friction term	N
q	Heat transfer term per unit time	W
T	Air temperature	K
f	Friction coefficient	/
g	Gravitational acceleration	m/s^2
ξ	Frictional work per unit time	W
κ	Specific heat ratio of air	/
C_{q}	Orifice discharge coefficient	/
α	Discharge coefficient of openings	/

References

1. Zhao Y, Yu ZF, Cai J, Lyu G, Liu JY, Yue L. Design concept and implementation path for badaling great wall station of Beijing-Zhangjiakou high-speed railway. Tunn Constr. 2020;40(7):929–40. (In Chinese).
2. Iyer RS, Kim DH, Kim HD. Propagation characteristics of compression wave in a high-speed railway tunnel. Phys Fluids. 2021;33(8):086104. [CrossRef].
3. Ricco P, Baron A, Molteni P. Nature of pressure waves induced by a high-speed train travelling through a tunnel. J Wind Eng Ind Aerodyn. 2007;95(8):781–808. [CrossRef].
4. Raghunathan RS, Kim HD, Setoguchi T. Aerodynamics of high-speed railway train. Prog Aerosp Sci. 2002;38(6–7):469–514. [CrossRef].
5. Ozawa S. Studies of micro-pressure wave radiated from a tunnel exit. Tokyo, Japan: Railway Technical Research Institute, Japan National Railways; 1979.
6. Choi JK, Kim KH. Effects of nose shape and tunnel cross-sectional area on aerodynamic drag of train traveling in tunnels. Tunn Undergr Space Technol. 2014;41:62–73. [CrossRef].
7. Cross D, Hughes B, Ingham D, Ma L. Enhancing the piston effect in underground railway tunnels. Tunn Undergr Space Technol. 2017;61:71–81. [CrossRef].
8. Kim JY, Kim KY. Experimental and numerical analyses of train-induced unsteady tunnel flow in subway. Tunn Undergr Space Technol. 2007;22(2):166–72. [CrossRef].

9. Baker CJ. A review of train aerodynamics part 1—fundamentals. Aeronaut J. 2014;118(1201):201–28. [CrossRef].
10. Liu M, Zhu C, Zhang H, Zheng W, You S, Campana PE, et al. The environment and energy consumption of a subway tunnel by the influence of piston wind. Appl Energy. 2019;246:11–23. [CrossRef].
11. An WG, Kong WH, Guang DQ, Lu YC, Wang Z, An WB. Evolution law of piston wind in subway tunnel and its influence on ventilation safety. Saf Environ Eng. 2023;30(5):84–92. (In Chinese).
12. Kim JY, Kim KY. Effects of vent shaft location on the ventilation performance in a subway tunnel. J Wind Eng Ind Aerodyn. 2009;97(5–6):174–9. [CrossRef].
13. Juraeva M, Jin Ryu K, Jeong SH, Song DJ. Influence of mechanical ventilation-shaft connecting location on subway tunnel ventilation performance. J Wind Eng Ind Aerodyn. 2013;119:114–20. [CrossRef].
14. Vardy AE. Unsteady airflows in rapid transit systems. Proc Inst Mech Engrs. 1980;194(32):341–56. [CrossRef].
15. Kim B, Ahn J, Kwon H. Numerical study of the effect of the tunnel hood on micro-pressure wave for increasing high-speed train operation speed. J Mech Sci Technol. 2024;38(2):721–33. [CrossRef].
16. Saito S. Alleviation of micro-pressure waves radiated from tunnel hoods. Tunn Undergr Space Technol. 2024;147:105703. [CrossRef].
17. Klaver EC, Kassies E. Dimensioning of tunnels for passenger comfort in the Netherlands. Edmunds, UK: Professional Engineering Publishing; 2000. p. 737–56.
18. Mei YG, Jia YX. Numerical investigation on pressure waves produced by a high-speed train passing through a tunnel with perforated wall. J China Railw Soc. 2013;35(12):95–100. (In Chinese).
19. Weng M, Xiong K, Liu F. Influence of the door opening on the pressure transient caused by the high-speed subway train passing through the double-track tunnel with the mid-partition wall. Tunn Undergr Space Technol. 2023;142:105417. [CrossRef].
20. Li N, Li T, Zhang J. Study on the influence of tunnel opening partition walls on the pressure wave characteristics and mitigation effects during train passage. Tunn Undergr Space Technol. 2026;172:107577. [CrossRef].
21. Xie J, Zhu F, Zhang M, Yao HD, Niu J. Numerical study on space-time distribution characteristics of pressure waves generated by a high-speed metro train operating along various lines of bifurcated tunnels. Phys Fluids. 2024;36(9):095152. [CrossRef].
22. Khaleghi M, Talaee MR. Analysis of unsteady airflow in a subway station influenced by train movement. Sci Technol Built Environ. 2020;26(2):210–8. [CrossRef].
23. Zhou D, Li S, Wu F, Yang M, Meng S, Meng S. The aerodynamic performance of a metro train passing through different shield transfer structures. Tunn Undergr Space Technol. 2024;144:105512. [CrossRef].
24. Woods WA, Pope CW. A generalised flow prediction method for the unsteady flow generated by a train in a single-track tunnel. J Wind Eng Ind Aerodyn. 1981;7(3):331–60. [CrossRef].
25. Pope CW. Gas dynamics and thermodynamics of unsteady flow in a railway tunnel [dissertation]. Milton Keynes, UK: The Open University; 1986.
26. Linic S, Ocokoljic G, Ristic S, Lucanin V, Kozic M, Rasuo B, et al. Boundary-layer transition detection by thermography and numerical method around bionic train model in wind tunnel test. Therm Sci. 2018;22(2):1137–48. [CrossRef].